Mao et al. Journal of Orthopaedic Surgery and Research (2025) 20:218
https://doi.org/10.1186/s13018-025-05596-4

Journal of Orthopaedic Surgery and Research

RESEARCH

Open Access

Decellularized tendon patch enhance biological and mechanical healing of large-to-massive rotator cuff tear in a rat chronic model: a comparison study of patch sterilization and storage methods

Yiyang Mao[1,2†], Yirui Wang[2,3†], Shen Liu[2,3], Zechun Liu[1,2], Pengling Yao[2,3], Buhua Sun[1,4*] and Can Chen[1,2,4*]

Abstract

Background Large-to-massive rotator cuff tears (L-M RCTs) usually requires a patch to reconstruction. Decellularized tendon patch (DTP) was a biomimetic and effective material for reconstructing L-M RCTs. However, the protocol for DTP sterilization and storage is variable, which may influence their performance. The objective of this study is to optimize the protocol of DTP sterilization and storage and fabricate an off-the-shelf DTP with superior efficacy in enhancing the healing of L-M RCTs.

Methods DTPs were sterilized by ethylene oxide (EO) or gamma irradiation (GR), then preserved using cryo-preservation (CP) or freeze-drying (FD), thus preparing four kinds of DTPs (EO/CP-DTP, EO/FD-DTP, GR/CP-DTP, GR/FD-DTP). After evaluating their histology, microstructure, biomechanics, biocompatibility, and tenogenic inducibility in-vitro, a total of 88 male SD rats with chronic L-M RCTs were randomly divided into 4 groups, and then reconstructed with one of the four DTPs. At postoperative week 4 or 8, the supraspinatus tendon-to-humerus complexes were harvested for gross, micro-CT, histological, and mechanical evaluations.

Results In-vitro results indicated that the four kinds of DTPs showed excellent biocompatibility, and EO/CP-DTP showed an orderly collagen arrangement and higher tensile properties than the other DTPs. More importantly, the EO/CP-DTP can induce more interacted stem cells toward tenogenic lineages as compared with the other kinds of DTPs. Micro-CT showed that bony footprint in the four groups showed similar value in bone morphological parameters without significant difference. Histologically, the two CP-sterilized DTPs presented significantly higher scores than the FD-sterilized DTPs, while the EO/CP-DTP group exhibited slightly higher scores compared to the GR/CP-DTP group. As for the mechanical strength of the supraspinatus tendon-to-humerus complexes, a significantly

†Yiyang Mao and Yirui Wang contributed equally to this work.

*Correspondence:
Buhua Sun
276165453@qq.com
Can Chen
chencanwow@foxmail.com

Full list of author information is available at the end of the article

higher failure load showed in the CP-sterilized DTPs when compared with the FD-sterilized DTPs at postoperative week 4 or 8.

Conclusion DTP should be sterilized by EO and preserved using CP, owing that this type of DTP well preserved the intrinsic bioactivity and mechanical properties as well as showed superior efficacy in enhancing the healing of L-M RCTs.

Level of evidence Basic Science Research; Animal Model.

Keywords Rotator cuff tears, Decellularized matrix, Tendon patches, Sterilization, Storage

Introduction

Rotator cuff tear (RCT) affect over 40% of patients older than 60 years, by inducing debilitating pain, shoulder disorder, and muscle weakness [1]. Although the overall results for arthroscopic repair of RCT have been favorable, incomplete enthesis regeneration, and gap formation at the bone-tendon (B-T) healing site can lead to structural and biomechanical weaknesses [2]. As a result, retear rates remain at 20–40%, with up to 94% for large-to-massive rotator cuff tears (L-M RCTs) [3–5]. To avoid retear of repaired L-M RCTs, one strategy is to improve the biomechanics of repair construct, and another is to enhance biological and function B-T healing [6–9]. To this clinical challenge, augmenting the repair of L-M RCTs using a patch has been proposed, considering the benefits of reducing tension, augmenting the friable and degenerative tendon end, providing an empty scaffold for tissue ingrowth [6, 7, 10, 11]. In clinical, the patches used for the repair of RCT, include acellular dermal allograft, dermal xenograft, small intestinal submucosa, synthetic patch [12–15], but concerns exist about healing or incorporation with native enthesis tissue, owing to their low biomimetics with native tendon; while the synthetic scaffolds have the additional concerns of biocompatibility and foreign-body reaction [16]. Therefore, an ideal patch for the repair of L-M RCTs should be capable of mimicking the extracellular matrix (ECM) of native tendon while providing sufficient biomechanics to reducing tension among the healing interface.

Decellularized biomaterials have been extensively utilized in the field of tissue reconstruction and repair [17–24], which may be an ideal patch for the reconstruction of RCTs, particularly, L-M RCTs. Until now, various types of decellularized patches, such as tendon matrix, dermal matrix, intestinal submucosa, pericardium matrix, have been developed for the reconstruction of RCTs [14, 25]. Among them, decellularized tendon patch (DTP) was considered as the most ideal biomaterial, owing to low immunogenicity and antigenicity, suitable for tenocytes attachment and proliferation, and high biomimetics to normal tendon in ultrastructure and composition [26–28]. In recent years, Juan Pan et al.'s study found that the DTP is suitable of reconstructing RCT and facilitating enthesis regeneration at the healing site [27]. Additionally, Guo-Ming Liu et al.'s study further determined that the DTP could be used to bridge rotator cuff defect in a rabbit L-M RCT model, and improve histological and biomechanical properties of the repaired RCT [28]. In the two studies, the DTP were freeze-dried and packaged in polythene wrappers for storage, and then sterilized with ethylene oxide (EO) before in-vivo application [27, 28]. In fact, there are many sterilization and storage methods for biomaterials, and different sterilization or storage methods could result in different influence on the structure and function of biomaterial [29–32]. Thus, for future clinical application of DTP, it is important to consider the impact of various sterilization methods and storage conditions on its properties.

The sterilization methods for biomaterials include gamma radiation (GR), EO, alcohol, ultraviolet rays and supercritical carbon dioxide, while GR or EO was the common method for the sterilization of decellularized biomaterials [29–32]. However, the decellularized implants sterilized using EO has a high risk of causing synovitis, while GR could lead to the decrease of biomechanical strength of the implant [33–35]. To date, no consensus exists on an appropriate protocol for DTP sterilization. The storage for decellularized materials includes cryo-preservation (CP), freeze-drying (FD), vapor phase liquid nitrogen, chemical disinfectant and normal temperature storage [36–38]. Among them, CP and FD are currently acknowledged as the most dependable and widely implemented ways for the storage of decellularized biomaterials [36–38]. The CP is more convenient but the associated cost is high, while FD storage is associated with greater ease of long-term storage and economic benefit. Nevertheless, studies have indicated that FD may lead to decreased allograft stiffness [39]. Until now, there are no controlled studies that investigate the difference of DTPs preserved using CP or FD.

In this study, the GR or EO was selected for patches sterilization, while CP or FD for storage, thus four kinds of combinative protocols were designed for DTP sterilization and storage. This study aimed to evaluate the influence of different sterilization and storage methods on the histology, microstructure, biomechanics, biocompatibility, and tenogenic inducibility of DTPs in-vitro, meanwhile biomechanically and histologically compare

L-M RCT repair at postoperative week 4 or 8 using the four types of DTPs: EO/CP-DTP, EO/FD-DTP, GR/CP-DTP, GR/FD-DTP. This study hypothesized that the EO/CP-DTP could enhance biological and biomechanical healing of the L-M RCTs in a rat model.

Materials and methods

Preparation of DTP

Human tendons were obtained from patients undergoing orthopedic amputation. The muscle and fascia were removed from the obtained tendons, which was then trimmed into a cylindrical shape along its long axis and immersed in a phosphate-buffered saline (PBS) containing 1% penicillin-streptomycin (Pen-Strep). After that, the trimmed tendons were immersed in 30 mL of PBS and sealed in a sterile 50 mL centrifuge tube. This tube was immediately submerged in liquid nitrogen for 2 min, followed by placement in a water bath at 37 °C for 10 min. This experimental procedure was repeated five times. Subsequently, the tissue was immersed in a 0.1% sodium dodecyl sulfate solution (Sigma) containing 1% penicillin-streptomycin (Gibico) at 37 °C for 4 h with agitation on a shaker. After washing the tissues with PBS at 4 °C for 2 h, the acquired DTPs were prepared for the following studies. The fresh tendon (FT) was used as control.

Different protocols for DTP sterilization and storage

These prepared DTPs were randomly divided into four groups and subjected to the following four different combinations of sterilization and storage: (1) EO sterilization followed by cryo-preservation (EO/CP group); (2) EO sterilization followed by freeze-drying storage (EO/FD group); (3) GR sterilization followed by cryo-preservation (GR/CP group); (4) GR sterilization followed by freeze-drying storage (GR/FD group).

EO sterilization: the DTPs were placed individually in centrifuge tubes, and sealed the tube with sealing film. Then the sealing film was punched by a 1mL syringe to make several small holes. After that, the tubes containing DTPs was subjected to low-temperature EO for 12 h sterilization.

GR sterilization: the DTPs were placed individually in centrifuge tubes, and sealed the tube with a sealing film. Then the sealing film was punched by a 1mL syringe to make several small holes. After that, the tubes containing DTPs was subjected to 15 kGy gamma irradiation for 24 h sterilization.

Cryo-preservation: the tubes containing DTPs were gradually frozen at a rate of 1 °C to 2 °C per minute, first placed in a 4 °C refrigerator for 20 min, then placed in a -20 °C refrigerator for 30 min, and finally placed in an -80 °C deep-freeze freezer for long-term cryo-preservation.

Freeze-drying storage: the tubes containing DTPs were placed in a vacuum freeze-dryer and pre-frozen for 30 min. They were then vacuum-frozen to -50-60℃ and subjected to negative pressure freeze-drying. When they were completely dried, the DTPs were sealed hermetically with a sealing film for storage at room temperature.

Histological, microstructural, and biomechanical assessments of the four DTPs

After 1 month of storage, the four DTPs (EO/CP-DTP, EO/FD-DTP, GR/CP-DTP, GR/FD-DTP) were captured for gross observation, then embedded by paraffin for histological assessments. The paraffin-embedded DTPs were sectioned into 5-μm slices and stained with 4',6-diamidino-2-phenylindole (DAPI), hematoxylin and eosin (H&E), masson's trichrome (MT), COL-1 and COL-3 immunohistochemical staining. In addition, the microstructure of the DTPs was observed with scanning electron microscopy (SEM) (S-3400 N; Hitachi, Japan).

The four kinds of DTPs and fresh tendons (FT) were trimmed to a length of 2 cm with a cross-sectional area of 5 mm × 3 mm using freezing microtome before mechanical test. The two ends of the four kinds of DTPs and FT were wrapped with gauze and secured within upper and lower clamps to prevent slippage during tensile testing. Specimens underwent mechanical testing in air at room temperature using an Instron 3343 System (USA). After preloading each specimen with a force of 0.1 N, they were subjected to failure loading at a rate of 4 mm/s. Failure load (N) and stiffness (N/mm) values were derived from the recorded load-deformation curves.

Biocompatibility and tenogenic inducibility of the four DTPs

The four kinds of DTPs were sectioned into a slice of 100 μm before evaluating their biocompatibility and tenogenic inducibility. For evaluating the biocompatibility of the four DTPs, bone marrow-derived stem cells (BMSCs) at a density of 1.2×10^4/cm2, Passage 3 were seeded onto DTPs or Fresh Tendon (FT, as controls) ($n = 3$). After 1, 3, 5, 7 and 9-day culture, cell proliferation on the DTPS or FT was quantified by CCK8 kit (70-CCK8100, MultiSciences, China). To assess the cytotoxicity of DTP on BMSCs, cell viability was evaluated using a Live/Dead assay kit (40747ES76, Yeasen, Shanghai, China) at 3 days post-seeding ($n = 5$). Green-stained (live cells) and red-stained (dead cells) were visualized using a fluorescence microscope with excitation wavelengths of 488 nm and 594 nm. Cell viability was calculated as follows: (live cells/total cells) × 100%. For evaluating the tenogenic inducibility of the four DTPs, BMSCs at a density of 1×10^6/cm2 were seeded on the DTPs or tissue culture polystyrene (TCP, as control). A 7-day quantitative real-time polymerase chain reaction

Table 1 Primer sequences were utilized for qRT-PCR gene expression analysis

Genes	Primer sequence	Species
SCX	Forward primer 5′-AACACGGCCTTCACTGCGCTG-3′ Reverse primer 5′-CAGTAGCACGTTGCCCAGGTG-3′	Rat
TNMD	Forward primer 5′-GTGGTCCCACAAGTGAAGGT-3′ Reverse primer 5′-GTCTTCCTCGCTTGCTTGTC-3′	Rat
GAPDH	Forward primer 5′-ATGGCCTTCCGTGTTCCTAC-3′ Reverse primer 5′-CAGCCCCAGCATCAAAGGT-3′	Rat

TNMD: tenomodulin, SCX: scleraxis, GAPDH: D-glyceraldehyde-3-phosphate dehydrogenase

(qRT-PCR) analysis was performed for expression of scleraxis (SCX), tenomodulin (TNMD), and GAPDH (D-glyceraldehyde-3-phosphate dehydrogenase). The primer sequences are listed in Table 1. To further assess the tenogenic inducibility, SCX expression in BMSCs was evaluated by immunofluorescence assay using the anti-SCX antibody (ab58655; Abcam).

Animal model and patch implantation

One shoulder surgeon (Yirui Wang) performed all of the surgical procedures. Intramuscular anesthesia was used with pentobarbital sodium (50 mg/kg, administered via intraperitoneal injection; Sigma) for all of the surgical procedures. Ampicillin (50 mg/kg) and ketorolac (3 mg/kg) were injected intramuscularly once daily until the third day after surgery.

A total of 88 male SD rats weighing 220–250 g, were utilized to establish a chronic L-M RCT repair model for this experiment. First, a tear of the supraspinatus tendon was created by cutting at its insertion. The teared end of supraspinatus tendon was sealed using a plastic drain to prevent spontaneous healing. For forming a chronic L-M RCT, the rats were managed for 6 weeks after the supraspinatus tendon tear with free-cage activity [40–43]. Those rats with chronic L-M RCT were randomly allocated into 1 of 4 DTPs for the reconstruction of RCT ($n = 22$ per group). At 6 weeks after supraspinatus tendon tear creation, meticulous adhesiolysis and scar tissue were removed for identifying the retracted tendon stump and greater tuberosity. Two bone tunnels for repair were formed in the greater tuberosity and proximal humerus, and No 3-polypropylene suture (Prolene) was passed through these tunnels, then the suture was passed through to the torn tendon. The two suture limbs on the bone side were passed through one end of the DTP. On the tendon side, one suture was passed through the tendon (just proximal to the suture for repair) to the other end of the DTP. The whole length of the patch covered the bone, bone-to-tendon interface, and the teared end of supraspinatus tendon. All rats were managed for an additional 4 or 8 weeks with free-cage activity and then humanely euthanized to harvest the supraspinatus tendon-to-humerus complex (STHC) for the following evaluation.

Evaluating biological and mechanical healing of L-M RCT

Morphological assessment: the supraspinatus tendon-to-humerus complexes were captured for observing the appearance of the repaired RCT.

Micro-CT ($n = 5$ per group): the humeral head of specimens with supraspinatus tendon were assessed using a Micro-CT with a 10.4 μm isotropic voxel resolution under 55 kV voltage (vivaCT 80, Scanco Medical, Switzerland). The bone volume fraction (bone volume/total volume; BV/TV) and trabecular bone number (Tb. N) were calculated for a ROI located at the greater tuberosity.

Histological evaluation ($n = 5$ per group): the specimens were fixed and embedded within paraffin, then sectioned into 5-μm slices for H&E and SO/FG staining. H&E-stained and SO/FG-stained images were used for fibrocartilage morphological evaluation, cellularity, and insertion continuity. The images were quantitatively analyzed by two blinded observers (Y. M and Z. L) by a modified histological scoring system [44, 45] as showed in Table 2. A higher score means improved RCT repair, with a score of 28 equivalent to a healthy rotator cuff insertion.

Biomechanical testing ($n = 6$ per group): After carefully dissecting the supraspinatus tendon and the attached humerus, the tendon end was secured in a screw clamp

Table 2 Histological score system for the fibrocartilage regeneration*

Individual items	Score			
	1	2	3	4
Cellularity	Marked	Moderate	Mild	Minimal
Presence of fibrocytes (%)	< 25	26–50	51–75	> 75
Fibrocartilage cells oriented parallel (%)	< 25	26–50	51–75	> 75
Collagen fibers oriented parallel (%)	< 25	26–50	51–75	> 75
Presence of cartilaginous matrix	Minimal	Mild	Moderate	Marked
Insertion integrity	C(+),R(-), F(-),T(-)	C(+),R(+), F(-),T(-)	C(+),R(+), F(+),T(-)	C(+),R(+), F(+),T(+)
Insertion continuity (%)	< 25	26–50	51–75	> 75

* 7 Individual outcomes on a scale of 1 to 4

C means "continuity", R means "regularity", F means "fibrocartilage", T means "Tidemark"

using sandpaper, while the humerus was fixed with resin and then firmly clamped with vice grip. The specimens were tested in air at room temperature using mechanical testing system (Instron 3343 System, USA). After preloaded with 0.1 N, the specimen was loaded to failure at a rate of 4 mm/s. Failure load (N) and stiffness (N/mm) were obtained from the recorded load deformation curve. During testing, 0.9% saline was applied to avoid specimen dehydration.

Statistical analysis

All quantitative data are expressed as mean ± standard deviation (SD). Student's t-test was employed for comparisons between two groups. One-way ANOVA with a post hoc test was utilized for comparisons involving more than two groups. P-value of less than 0.05 was considered statistically significant. Statistical analyses were conducted using SPSS version 21.0 software (SPSS, USA).

Results

Histological, microstructural, and biomechanical properties of the four DTPs

As showed in Fig. 1A, Fresh tendon (FT, as control) was white, showing a smooth surface with intact edges, good elasticity and tensile strength. The four DTPs remained intact with no obvious fiber ruptures, and the edges of the DTPs displayed some rough fibers. In addition, the four DTPs also exhibited good elasticity and the collagen fibers were aligned along the longitudinal axis.

As showed in Fig. 1B, the H&E or DAPI-stained images of the four DTPs showed no extensive cell nuclei, indicating the successful decellularization. MT images demonstrated that the FT had tightly ordered collagen fibers, arranged parallel to the tendon axis with excellent continuity, no visible fiber ruptures, and numerous blue-purple tenocytes were interspersed among the collagen fibers aligning with their direction and distributed uniformly (Fig. 1C). The collagen fibers in the EO/CP-DTP displayed a regular arrangement, predominantly aligned along the tendon axis in a wavy parallel pattern. In addition, the fibers exhibited good continuity, with only minor ruptures. In the EO/FD-DPT, the collagen fibers displayed a poorly ordered arrangement, with fibers following the tendon axis in a wavy pattern, accompanied by fusion disorders and noticeable ruptures. In the GR/CP-DPT, the collagen fibers generally exhibited a regular arrangement, aligned along the tendon axis in a wavy parallel pattern, but with poorer continuity and noticeable ruptures. The collagen fibers in the GR/FD-DPT exhibited a disordered arrangement with numerous discontinuities observed in several areas and the tendon bundles appeared indistinct.

The COL-1 and COL-3 immunohistochemical staining showed that the FT and the four DTPs were positive for the expression of COL-1 and COL-3 (Fig. 1C). Following decellularization, part of ECM substances was removed, leaving primarily type I collagen, which resulted in strong positive expression of COL-1 in the four DTPs. Additionally, the reticular structure of type III collagen was exposed, leading to increased positive expression of COL-3 compared to the FT. Staining of type I and type III collagen in GR/FD-DPT was reduced and exhibited an irregular distribution, indicating that the content of these collagens was reduced and the fiber arrangement was damaged (Fig. 1C).

As showed in the SEM images (Fig. 1D), the collagen fibers in the FT were arranged in an orderly, interlaced manner, forming relatively thick tendon fiber bundles, with no significant loose. In the EO/CP-DPT, collagen fibers were arranged in a regular parallel manner, with no significant loose and overlapping between the fibers, while the collagen fibers in the EO/FD-DPT were arranged in a general manner, which were roughly parallel with partial overlapping. In the GR/CP-DPT, collagen fibers were generally arranged in a parallel manner and appeared slightly swollen, with some fibers curling and overlapping. The collagen fibers of GR/FD-DPT were roughly parallel with partial overlapping and some fibers were curled and intertwined.

Biomechanical characteristics of the four DTPs

Using biomechanical test (Fig. 2A), EO/CP-DTPs showed similar values in failure load and stiffness to the FT without significant differences ($P > 0.05$). In addition, the CP-stored DTPs showed significantly higher failure load and stiffness than the FD-stored DTPs ($P < 0.05$), while the failure load and stiffness of the EO/CP-DTPs were slightly larger than the GR/CP-DTPs without significant differences ($P > 0.05$) (Fig. 2B). The experiment demonstrated that CP-stored DTPs exhibited relatively superior tensile properties to FD-stored DTPs.

Biocompatibility and tenogenic inducibility of the four DTPs

BMSCs proliferation in the FT or the four DTPs was evaluated using the CCK-8 assay. The two CP-sterilized DTPs presented similar proliferative profiles with the FT, and the CP-DTPs showed slightly higher proliferative profiles when compared to the FD-DTPs (Fig. 3A).

The Live/Dead assay showed that most BMSCs were stained fluorescent green (living cells), with very few red (dead cells). Quantitative analysis indicated that BMSCs viability on the EO/CP-DTPs, EO/FD-DTPs and GR/CP-DTPs showed similar values to the TCPs without significant differences ($P > 0.05$). However, GR/FD-DTPs exhibited lower cell viability than the other groups ($P < 0.05$ for all) (Fig. 3B).

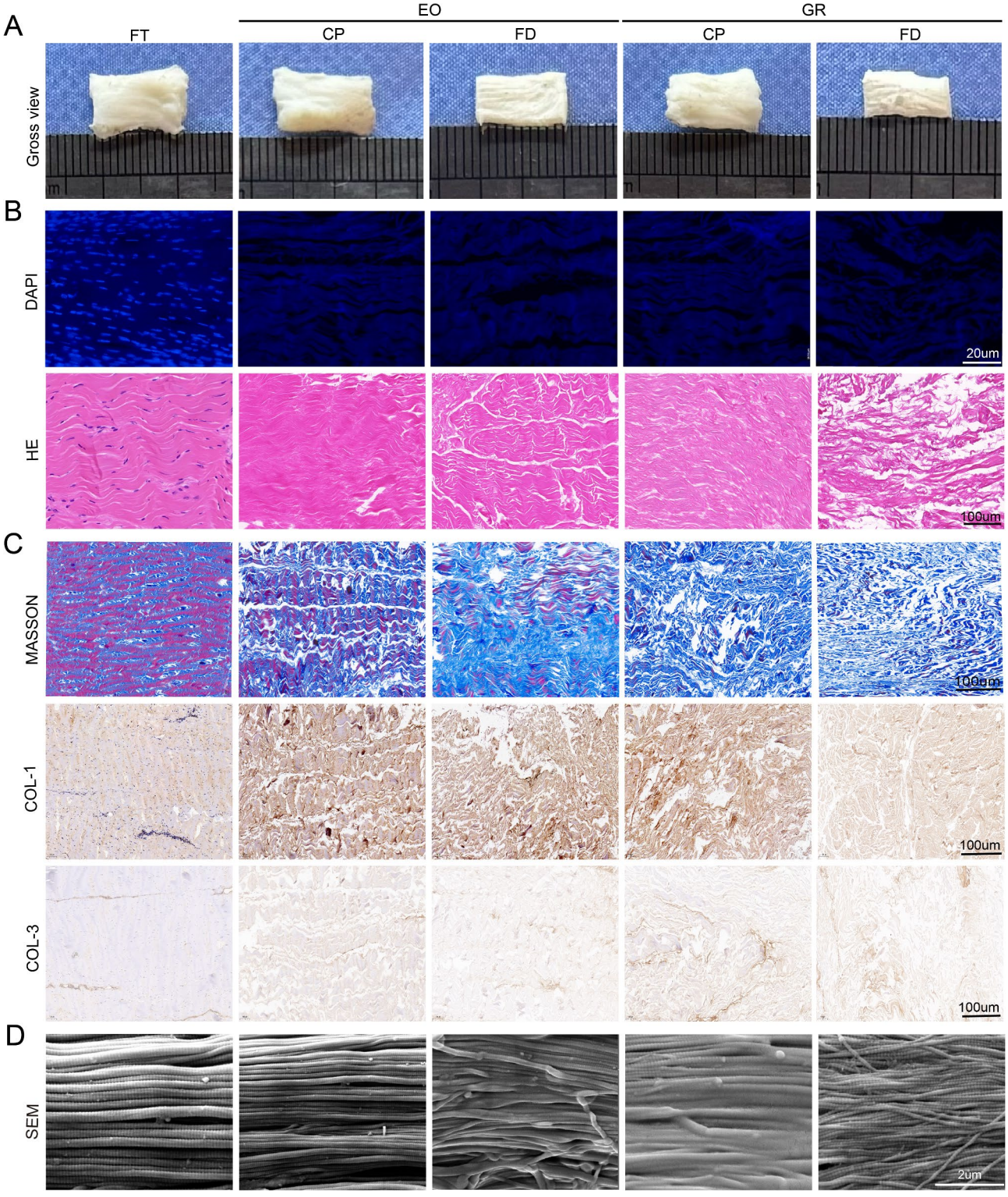

Fig. 1 (**A**) Macroscopic observation of the Fresh Tendon (FT) and the DTPs. (**B**) 4′,6-diamidino-2-phenylindole (DAPI), Hematoxylin and eosin (H&E) staining of the FT and the DTPs. (**C**) MASSON staining, Collagen I and collagen III immunohistochemical staining of the FT and the DTPs. (**D**) SEM for evaluating the microstructure of the FT and the DTPs

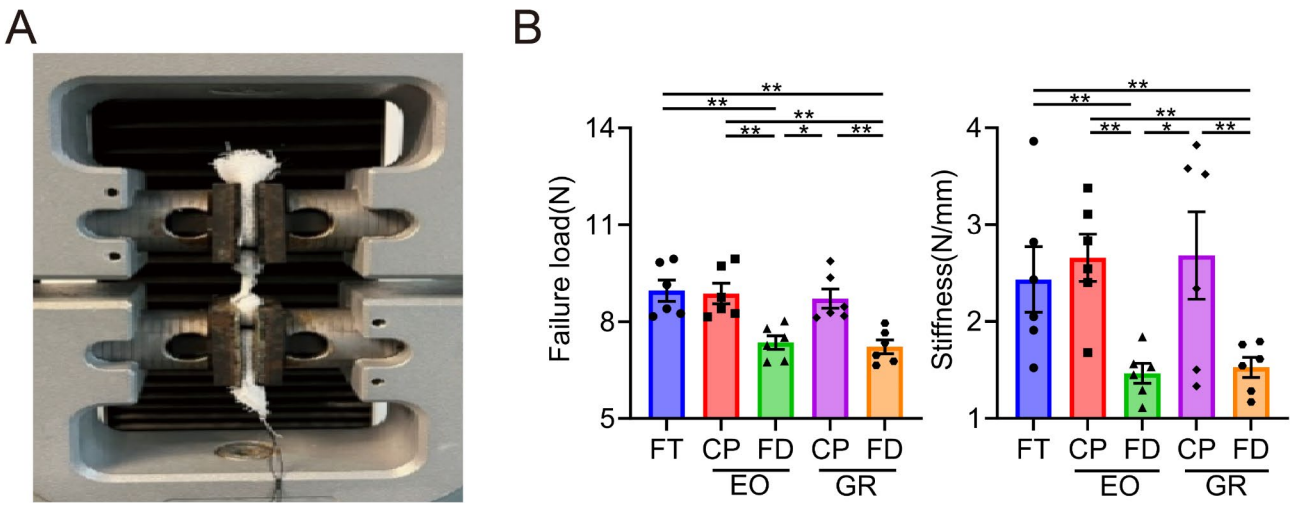

Fig. 2 Biomechanical testing. (**A**) The harvested specimens were securely mounted onto a metallic clamp. (**B**) Failure load and stiffness of the Fresh Tendon (FT) and the DTPs. $n = 6$ for each group. All values are presented as means ± standard deviation (*$P < 0.05$, **$P < 0.01$)

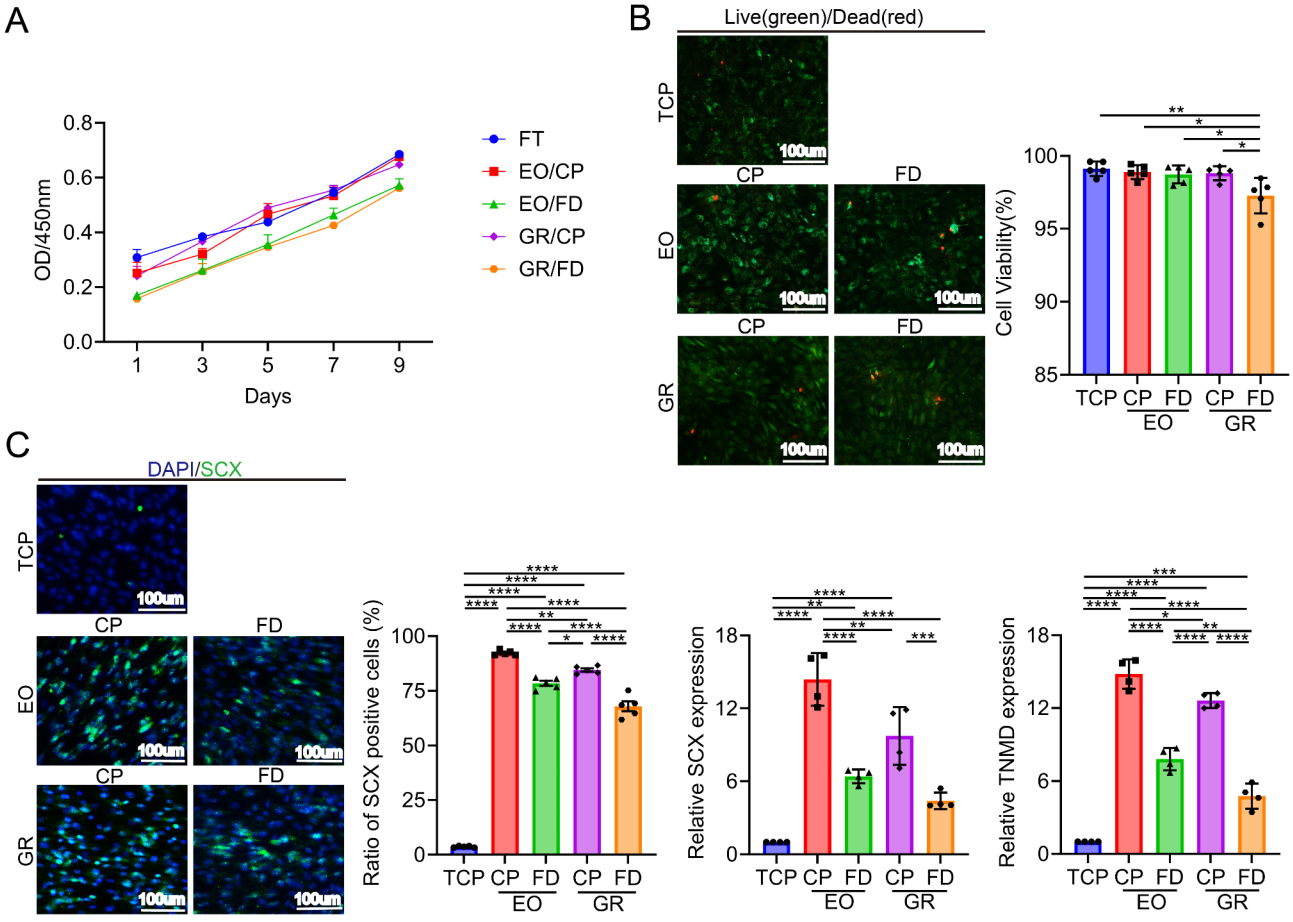

Fig. 3 (**A**) Comparative cell proliferation assay of BMSCs seeded on the Fresh Tendon (FT) and on the DTPs. (**B**) Live/dead cell analysis for the TCPs and the DTPs, representative images show the live (green) and dead (red) BMSCs in the TCPs and the DTPs and in the viability analysis for the cells on the TCPs and the DTPs. (**C**) SCX and TNMD expression in the BMSCs on the surface of TCPs and the DTPs after 7 d of coculture. All values are presented as mean ± SD (ns, $P > 0.05$. *$P < 0.05$. **$P < 0.01$. ***$P < 0.001$. ****$P < 0.0001$). TCPs, tissue culture polystyrene; SCX, scleraxis; TNMD, tenomodulin

The qRT-PCR and immunofluorescent assay results showed that the BMSCs cultured on the DTPs expressed significantly higher tenogenic genes (SCX and TNMD) than the TCPs. While the EO/CP-DTPs showed significantly higher tenogenic genes (SCX and TNMD) when compared to the other groups ($P < 0.05$ for all) (Fig. 3C).

Gross observations of the repaired L-M RCT specimens

No animals died during or after surgery. No postoperative infection happened to these animals. From the gross images of STHC, supraspinatus muscle and tendon showed no obvious muscle atrophy and fatty infiltration, the tendon end was tightly connected to the humerus, the grafted patch was disappeared at the healing site. In the shoulder joint, no significant adhesions, synovial hyperplasia and osteoarthritis were observed (Fig. 4).

Subchondral bone morphology at supraspinatus tendon footprint

From the micro-CT images, visible bone was formed at the greater tuberosity where the fibrocartilage tissue and subchondral bone were resected during operation (Fig. 5A). BV/TV and Tb.N increased with the extension of postoperative time, and showed no significant difference among the four groups at 4 or 8 weeks after operation. The mean value of the EO/CP-DTPs was slightly higher than the other groups ($P > 0.05$ for all) (Fig. 5B). The results indicated that the four DTPs showed no significant difference in promoting the formation and remodeling of subchondral bone.

Fibrocartilage regeneration at the healing site

Histological analysis utilizing H&E and SO/FG staining revealed that the ruptured supraspinatus tendon was effectively bridged by regenerated fibrocartilage accompanied by new bone formation at the proximal humerus across all groups at postoperative weeks 4 and 8 (Fig. 6A). At week 8, the EO/CP-DTP demonstrated a significant presence of collagen fibers arranged in close alignment with the stress direction at the bone-tendon interface, ensuring firm attachment of the supraspinatus tendon to the underlying bone tissue. The GR/CP-DTP showed a regular distribution of collagen fibers aligned along this stress direction, interspersed with visible purplish-red fibroblasts. In contrast, both the EO/FD-DTP and the GR/FD-DTP presented numerous deeply stained purplish-red fibroblasts at the healing interface without any discernible pattern. Histological score revealed that the CP-sterilized DTPs exhibited superior fibrocartilage formation than the FD-sterilized DTPs ($P < 0.05$), while EO/FD-DTP showed slightly higher scoring value than the GR/FD-DTP without significant difference ($P > 0.05$) (Fig. 6B).

Biomechanical testing

During biomechanical testing (Fig. 7), all specimens ruptured at the surgical repair site. The failure load and stiffness of the SSTH complex in all groups demonstrated a progressive increase with time. The CP-stored DTPs showed significantly higher failure load than the FD-stored DTPs ($P < 0.05$), while the stiffness value of the EO/CP-DTPs was slightly higher than the other groups without significant differences ($P > 0.05$ for all).

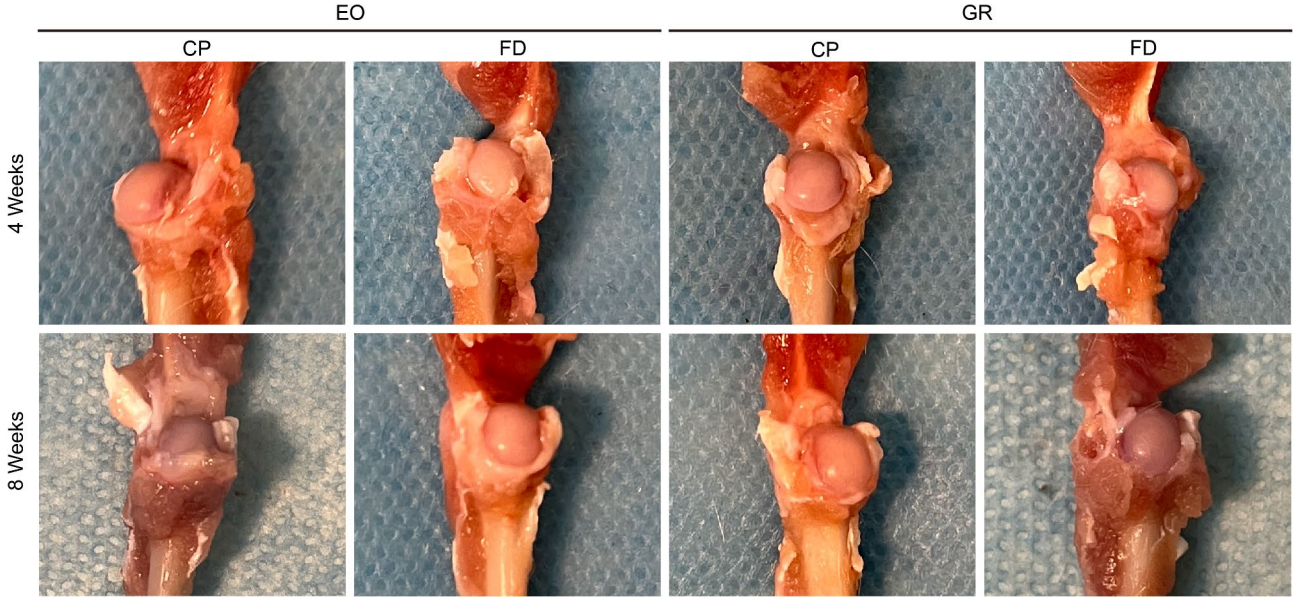

Fig. 4 Gross observations on STHC at postoperative weeks 4 and 8, SSTH: Supraspinatus humeral complex

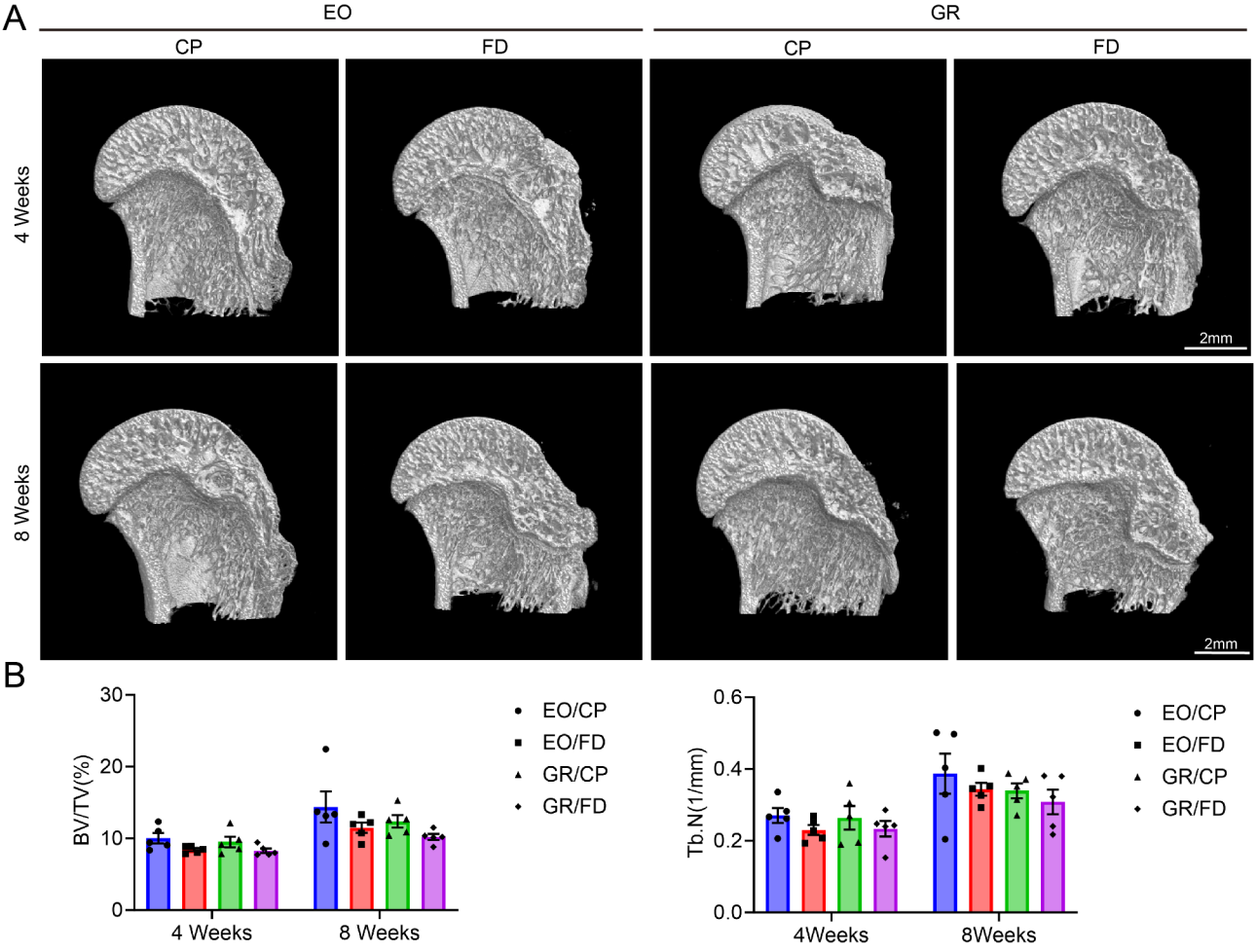

Fig. 5 (**A**) Representative Micro-CT images of the head of humerus at postoperative weeks 4 and 8. (**B**) Comparison of the bone volume fraction (bone volume/total volume; BV/TV), trabecular bone number (Tb.N). $n = 5$ for each group per time point. All values presented as means ± standard deviation (*$P < 0.05$)

Discussions

The findings of this study confirmed that the DTP sterilized by EO and preserved using CP exhibits a highly biomimetic structure, superior biomechanics, excellent biocompatibility and tenogenic inducibility. In addition, this kind of DTP showed excellent biological performance in enhancing the repair of L-M RCT. These results indicated that the prepared DTP should be sterilized by EO and then preserved using CP for avoiding the structural damage and bioactivity loss.

An ideal protocol for DTP sterilization and storage should be capable of minimizing the risk of disease transmission, reducing the immunogenicity of biomaterials, preserving their physical and chemical properties as well as biological activity, and avoiding toxicity introduction [29, 31, 38]. The sterilization is the first step on biomaterials preparation, infections could cause rejection of implants or eventually the death of patient, thus the elimination of microorganisms, such as bacteria, spores, protozoa, fungi, and virus, are essential to reach an acceptable level of safety on sterilization [46]. The sterilization method for DTP can be assessed through the following steps: first, verifying complete sterilization through a sterility test; second, detect any toxic or harmful substances using a cytotoxicity test; and finally, evaluate whether changes in the physical, chemical and biological properties during sterilization. Once these criteria are met, the sterilized DTP can be prepared for the following in-vivo application. Common sterilization methods for biological materials include GR, EO, alcohol, ultraviolet rays and supercritical carbon dioxide [47–50]. In our study, only two most commonly used sterilization methods (GR and EO) were selected and comparatively evaluated. In the EO group, the collagen fibers in the DTPs displayed regular and uniform alignment, with few interruptions in continuity. In contrast, the DTPs of the GR group exhibited slight disarray in the morphology of collagen fibers, with noticeable interruptions in continuity. Biomechanical testing revealed that the EO group exhibited superior biomechanical

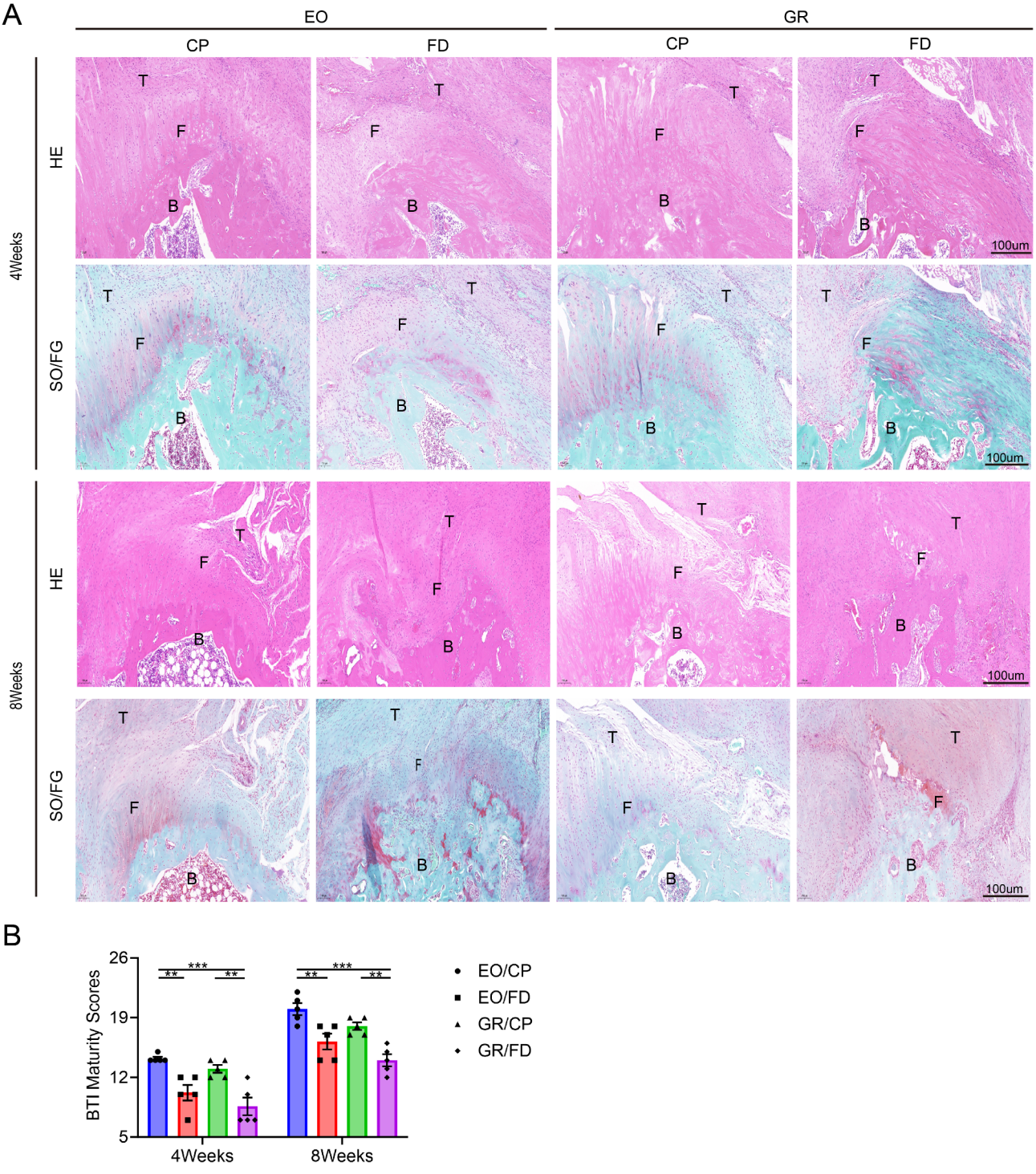

Fig. 6 Histological analyses of regenerated fibrocartilage during RC healing. (**A**) RC insertion sections stained with hematoxylin and eosin (H&E), SO/FG. B: bone, F: fibrocartilage, T: tendon. (**B**) BTI Maturity scores for the regenerated fibrocartilage (**P < 0.05*)

properties compared to the GR group. Conversely, the BMSCs cocultured the EO-sterilized DTPs proliferated slower than the cells on the GR-sterilized DTPs, which may result from some residues of EO [33]. Nonetheless, live-dead staining assays showed the cell viability of the four kinds of DTPs was larger than 95%, indicating high biocompatibility. EO has the capability of sterilization due to disruption of microbial metabolic activity to kill bacteria and their spores, therefore biomaterials sterilized by EO showed limited change in mechanical and

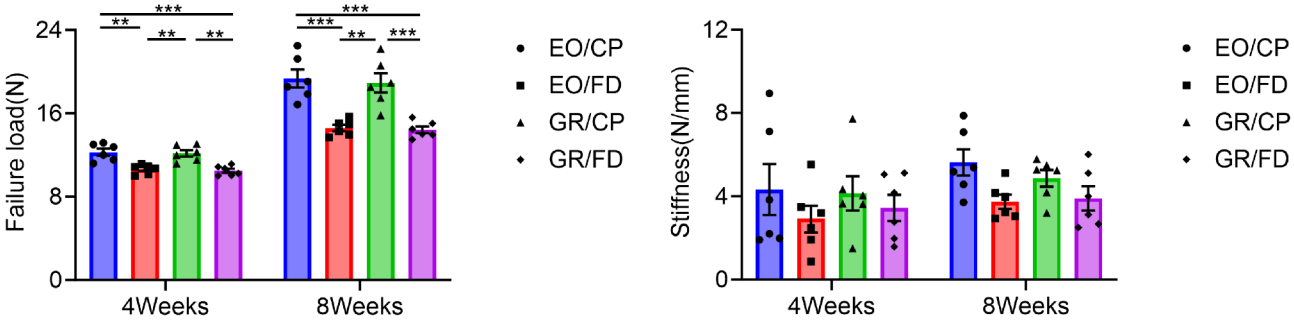

Fig. 7 Failure load and Stiffness of specimens. $n = 6$ for each group per time point. All values presented as means ± standard deviation (*$P < 0.05$, **$P < 0.01$, ***$P < 0.001$)

structural properties. By the contrast, GR has the ability of sterilization by protein denaturation, thus gamma irradiated biomaterials showed some changes in physical and chemical properties more or less [32]. As showed in this study, the structural integrity of GR-sterilized DTPs was compromised more seriously than that of the EO-sterilized DTPs, resulting in poor histological characteristics in the GR-sterilized DTPs compared to the EO-sterilized DTPs. In addition, the tenogenic inducibility of EO-sterilized DTPs was preserved well than the GR-sterilized DTPs, indicating that part of the tenogenic stimulators in the GR-sterilized DTPs were inactivated owing to gamma irradiation. For the same material, low-dose radiation can enhance the tensile strength and stiffness, whereas high doses may cause material degradation, resulting in reduced tensile strength and stiffness [48]. This study utilized a low dose of 15 kGy gamma irradiation for DPT sterilization, which may explain the slightly higher stiffness observed in the GR-sterilized DTPs compared to the EO-sterilized DTPs. Although there is no definitive superiority or inferiority of EO or GR-sterilized DTPs through structure and mechanical evaluation, the experiments of tenogenic inducibility demonstrated that EO-sterilized DTPs preserved better biological activity than the GR-sterilized DTPs. Therefore, the recommended sterilization method for DTP is EO.

As for the storage of sterilized DTP, it can be stored using a CP method or FD method. The FD method was more convenient for storage, because these FD-stored DTP can be kept at room temperature, while CP-stored DTP should be stored in a deep-freezing environment, which needs an expensive refrigeration facility. In previous studies about anterior cruciate ligament allografts, the FD-stored allografts showed more decrease in immune substances as compared with CP-stored allografts, thus harboring low immunogenicity [35, 51–53]. Based on that, the sterilized DTPs should be stored using FD method for reducing immunogenicity. While the FD procedure has some disadvantages, such as decreasing the stiffness of the allograft [54, 55], which may impact the mechanical performance of the DTP in-vivo. In our result, in-vitro mechanical tests indeed determined that rehydrated FD-stored DTP has significantly lower value of failure load and stiffness than CP-stored DTP. While in-vivo experiments revealed that RCT repair was significantly poorer in the FD-stored DTPs compared to the GR-stored DTP. These results indicated that the sterilized DTPs should be stored by CP method. For the inferiority of FD-stored DTPs on RCT repair, the reasons may be that: (1) based on published literatures, fascia lata autograft or biodegradable biomaterials-derived patch after reconstructing L-M RCTs undergo sequential processes, including infiltration and polarization of macrophages, revascularization, repair associated cells proliferation, patch repopulation, and eventual ligament engraftment [14, 56]. The collagen fibers of FD-stored DTPs in the SEM images were dense and disorganized, which was not convenient for endogenous cell migration, thus influencing the RCT repair. (2) the bioactive substances within the FD-stored DTPs may be denatured, likely due to structural and biomechanical alterations resulting from dehydration, room temperature, and rehydration. Our results determined that the FD-stored DTPs presented lower tenogenic inducibility than the CP-stored DTPs in-vitro, indicating part of bioactive substances within the FD-stored DTPs have lost bioactivities, thus showing poor quality in RCT repair.

In recent years, studies have shown that biological patches play a key role in improving tendon healing quality and reducing retear rates [57], which aligns well with the objectives of this study exploring the application of DTP as a biomimetic scaffold. Although imaging techniques such as MRI are widely used for postoperative evaluation, their ability to reflect tendon pathological conditions may have limitations [58], further supporting the necessity of a multidimensional evaluation of repair outcomes through histology and biomechanics in this study. Additionally, the efficacy differences between various surgical techniques, such as arthroscopic and open repair, have been systematically analyzed [59], and the potential of biological patches to enhance repair, regardless of the surgical method, is well recognized, providing

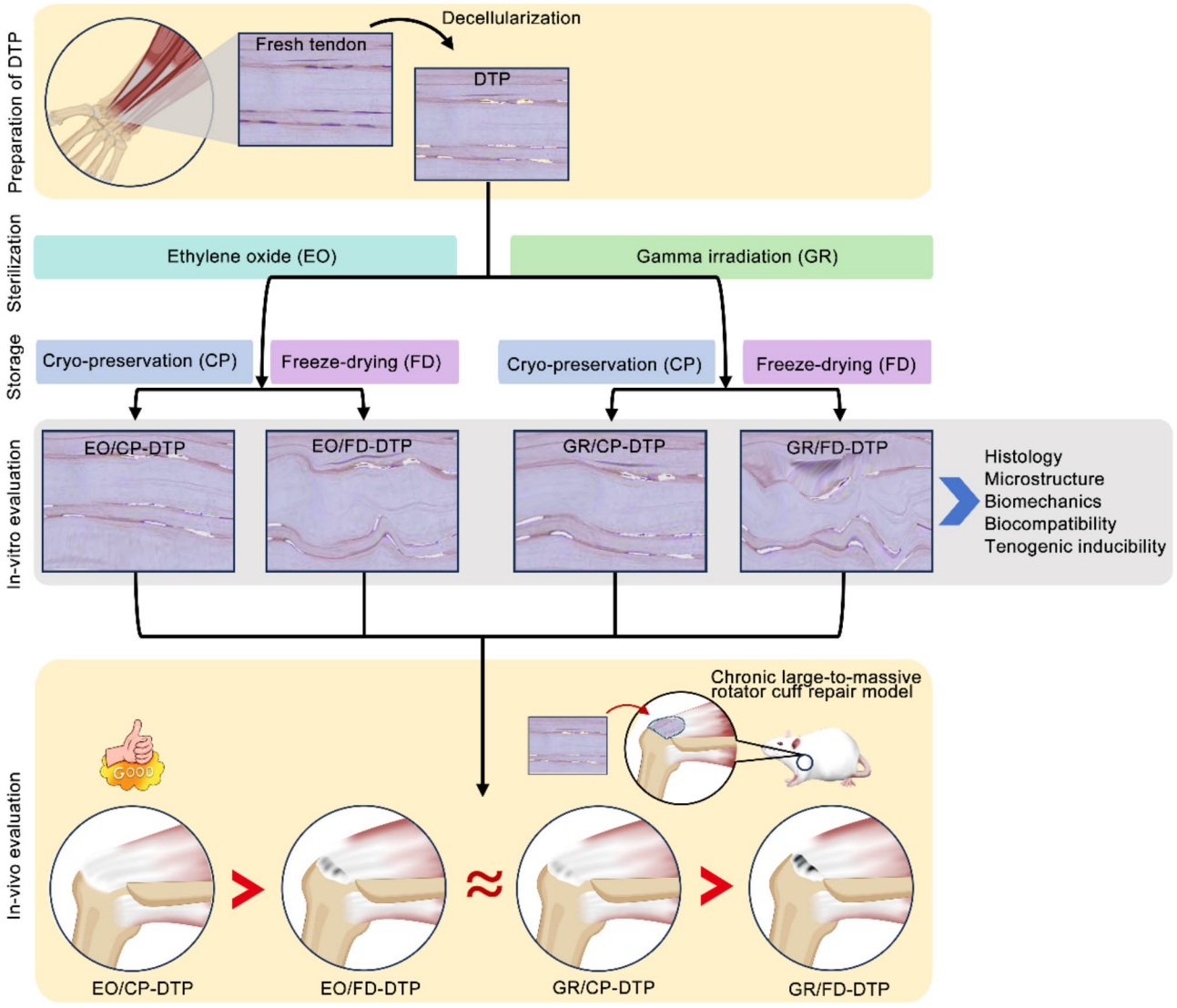

Fig. 8 Overview of the experiments

a theoretical basis for focusing on the optimization of DTP in this study. It is worth noting that the incomplete correlation between imaging success and clinical functional improvement [60] emphasizes the importance of comprehensive assessment. This study fully validates DTP, especially the combination of EO sterilization and CP preservation, as an ideal choice for enhancing the repair of L-M RCTs through maturity scoring, mechanical strength testing, and cell viability analysis.

Nevertheless, there are several limitations to our study. First, rats were used as the animal model for optimizing the protocol of DTP sterilization and storage, there are significant differences between rodent and human in rotator cuff anatomy, biomechanics, and repair processes. Thus, it is not rigorous to directly translate our results into human LM RCT reconstruction. Secondly, this study determined that the EO/CP-DTP enhance mechanical and biological healing of LM RCT in a rat chronic model, as shown by the better fibrocartilage regeneration and tensile resistance. However, the mechanism of why EO/CP-DTP is better than the other three kinds of DTPs is not clear and should be further investigated. Thirdly, before mechanical testing and in-vivo application, the CP-stored DTPs were preserved by CP method for 1 month, while the FD-stored DTPs were freeze-dried and then stored at room temperature for 1 month. In clinical setting, the storage duration of these DTPs varies, depending on the date of patient operation. Next step, a study should be designed to investigate negative influences of the storage duration on the in-vivo performance of the DTPs. Despite these limitations, this study comparatively evaluated the four kinds of sterilization and storage protocols for DTP concerning their histology, microstructure, biomechanics, biocompatibility,

and tenogenic inducibility in-vitro as well as their efficacy in RCT repair in-vivo, which may provide meaningful reference for selecting the DTP sterilization and storage method in clinical setting.

Conclusion

In this study (Fig. 8), we found that DTPs sterilized using EO and preserved through CP exhibits a highly biomimetic structure, superior biomechanics, excellent biocompatibility and tenogenic inducibility as well as preferable efficacy in enhancing mechanical and biological healing of L-M RCT in a rat chronic model. Consequently, EO combined with CP is considered the optimal protocol for DTP sterilization and storage in clinical setting.

Acknowledgements
This research was supported by the Fundamental Research Funds for the Central Universities of Central South University (2022XQLH182, 2024ZZTS0872 and 2024ZZTS0927).

Author contributions
Conception and design: YM, YW, BS, and CC; Methodology and data collection: YM, YW, SL, and ZL; Contributed data/analysis tools and formal analysis: YW, SL, ZL, and PY; Investigation: YW and SL; Data curation: YM and ZL; Writing—original draft preparation: YM and YW; Writing—review and editing: YM, YW,BS, and CC; Visualization: PY; Funding acquisition: BS and CC. All authors reviewed the manuscript.

Data availability
Data is provided within the manuscript.

Declarations

Ethical approval
The experimental protocol for the use of Sprague-Dawley (SD) rats in this study was approved by the Animal Ethics Committee of Xiangya Hospital, Central South University. In addition, the tendons were harvested from two amputation patients with limb damage, and authorized by Clinical Ethics Committee of Xiangya Hospital, Central South University.

Competing interests
The authors declare no competing interests.

Author details
[1]Department of Orthopedics, Xiangya Hospital, Central South University, No. 87 Xiangya Road, Kaifu District, Changsha City, Hunan Province 410008, China
[2]Key Laboratory of Organ Injury, Aging and Regenerative Medicine of Hunan Province, Changsha, Hunan 410008, China
[3]Department of Sports Medicine, Xiangya Hospital, Central South University, No. 87 Xiangya Road, Kaifu District, Changsha City, Hunan Province 410008, China
[4]National Clinical Research Center for Geriatric Disorders, Xiangya Hospital, Central South University, Changsha, Hunan 410008, China

Received: 10 January 2025 / Accepted: 10 February 2025
Published online: 01 March 2025

References

1. Colvin AC, Egorova N, Harrison AK, Moskowitz A, Flatow EL. National trends in rotator cuff repair. J Bone Joint Surg Am. 2012;94:227–33. https://doi.org/10.2106/jbjs.J.00739.
2. Gulotta LV, Nho SJ, Dodson CC, Adler RS, Altchek DW, MacGillivray JD. Prospective evaluation of arthroscopic rotator cuff repairs at 5 years: part I–functional outcomes and radiographic healing rates. J Shoulder Elb Surg. 2011;20:934–40. https://doi.org/10.1016/j.jse.2011.03.029.
3. Koh KH, Kang KC, Lim TK, Shon MS, Yoo JC. Prospective randomized clinical trial of single- versus double-row suture anchor repair in 2- to 4-cm rotator cuff tears: clinical and magnetic resonance imaging results. Arthroscopy. 2011;27:453–62. https://doi.org/10.1016/j.arthro.2010.11.059.
4. Tashjian RZ, Hollins AM, Kim HM, Teefey SA, Middleton WD, Steger-May K, et al. Factors affecting healing rates after arthroscopic double-row rotator cuff repair. Am J Sports Med. 2010;38:2435–42. https://doi.org/10.1177/0363546510382835.
5. Toussaint B, Schnaser E, Bosley J, Lefebvre Y, Gobezie R. Early structural and functional outcomes for arthroscopic double-row transosseous-equivalent rotator cuff repair. Am J Sports Med. 2011;39:1217–25. https://doi.org/10.1177/0363546510397725.
6. Bailey JR, Kim C, Alentorn-Geli E, Kirkendall DT, Ledbetter L, Taylor DC, et al. Rotator Cuff Matrix Augmentation and Interposition: a systematic review and Meta-analysis. Am J Sports Med. 2019;47:1496–506. https://doi.org/10.1177/0363546518774762.
7. Yang J, Kang Y, Zhao W, Jiang J, Jiang Y, Zhao B, et al. Evaluation of patches for rotator cuff repair: a systematic review and meta-analysis based on animal studies. Bioact Mater. 2022;10:474–91. https://doi.org/10.1016/j.bioactmat.2021.08.016.
8. Papalia R, Franceschi F, Zampogna B, D'Adamio S, Maffulli N, Denaro V. Augmentation techniques for rotator cuff repair. Br Med Bull. 2013;105:107–38. https://doi.org/10.1093/bmb/lds029.
9. Longo UG, Lamberti A, Khan WS, Maffulli N, Denaro V. Synthetic augmentation for massive rotator cuff tears. Sports Med Arthrosc Rev. 2011;19(4):360–5. https://doi.org/10.1097/JSA.0b013e318224e359.
10. Sandhu H, Hackett L, Tumpalan JF, Lam PH, Murrell GAC. Synthetic polytetrafluoroethylene patches for irreparable rotator cuff tears-how are they doing at 5 years? J Shoulder Elb Surg. 2023;32:e106–16. https://doi.org/10.1016/j.jse.2022.08.016.
11. Dommer LM, Chlasta A, Rojas JT, Hayoz A, Schär M, Zumstein MA. Massive rotator cuff tears with short tendon length can be successfully repaired using synthetic patch augmentation. J Shoulder Elb Surg. 2023;32:2089–96. https://doi.org/10.1016/j.jse.2023.03.037.
12. Yanke A, Dandu N, Credille K, Damodar D, Wang Z, Cole BJ. Indications and technique: Rotator Cuff Repair Augmentation. J Am Acad Orthop Surg. 2023;31:1205–10. https://doi.org/10.5435/jaaos-d-23-00101.
13. Sclamberg SG, Tibone JE, Itamura JM, Kasraeian S. Six-month magnetic resonance imaging follow-up of large and massive rotator cuff repairs reinforced with porcine small intestinal submucosa. J Shoulder Elb Surg. 2004;13:538–41. https://doi.org/10.1016/j.jse.2004.03.005.
14. Na Y, Jue H, Xia T, Xue X, Sun L, Chen J, et al. Histologic and biomechanical comparison of fascia lata autograft, acellular dermal xenograft, and synthetic patch for bridging massive rotator cuff tear in a rabbit model. Asia Pac J Sports Med Arthrosc Rehabil Technol. 2024;36:28–39. https://doi.org/10.1016/j.asmart.2024.01.007.
15. Gögele C, Schwarz S, Ondruschka B, Hammer N, Schulze-Tanzil G. Decellularized Iliotibial Band recolonized with allogenic homotopic fibroblasts or bone marrow-derived mesenchymal stromal cells. Methods Mol Biol. 2018;1577:55–69. https://doi.org/10.1007/7651_2017_30.
16. Hakimi O, Mouthuy PA, Carr A. Synthetic and degradable patches: an emerging solution for rotator cuff repair. Int J Exp Pathol. 2013;94:287–92. https://doi.org/10.1111/iep.12030.
17. Wainwright DJ. Use of an acellular allograft dermal matrix (AlloDerm) in the management of full-thickness burns. Burns. 1995;21:243–8. https://doi.org/10.1016/0305-4179(95)93866-i.
18. Mancuso LA, Lassaline M, Scherrer NM. Porcine urinary bladder extracellular matrix grafts (ACell Vet® corneal discs) for keratomalacia in 17 equids (2012–2013). Vet Ophthalmol. 2016;19:3–10. https://doi.org/10.1111/vop.12240.
19. Vrankovic D, Mrcela T, Mursic B, Splavski B, Dmitrovic B, Mrcela M, et al. Physical and histologic properties of substitutes used for the anterior fossa region dural repair. Skull Base Surg. 1999;9:9–13. https://doi.org/10.1055/s-2008-1058167.
20. Ortiz JA. Clinical outcomes in breast Reconstruction patients using a sterile Acellular dermal matrix allograft. Aesthetic Plast Surg. 2017;41:542–50. https://doi.org/10.1007/s00266-017-0817-z.

21. Brigido SA, Carrington SC, Protzman NM. The Use of Decellularized Human Placenta in full-thickness Wound Repair and Periarticular Soft tissue Reconstruction: an update on Regenerative Healing. Clin Podiatr Med Surg. 2018;35:95–104. https://doi.org/10.1016/j.cpm.2017.08.010.
22. Milan PB, Lotfibakhshaiesh N, Joghataie MT, Ai J, Pazouki A, Kaplan DL, et al. Accelerated wound healing in a diabetic rat model using decellularized dermal matrix and human umbilical cord perivascular cells. Acta Biomater. 2016;45:234–46. https://doi.org/10.1016/j.actbio.2016.08.053.
23. Ferrando A, Kingston R, Delaney RA. Superior capsular reconstruction using a porcine dermal xenograft for irreparable rotator cuff tears: outcomes at minimum two-year follow-up. J Shoulder Elb Surg. 2021;30:1053–9. https://doi.org/10.1016/j.jse.2020.08.020.
24. Smith MJ, Bozynski CC, Kuroki K, Cook CR, Stoker AM, Cook JL. Comparison of biologic scaffolds for augmentation of partial rotator cuff tears in a canine model. J Shoulder Elb Surg. 2020;29:1573–83. https://doi.org/10.1016/j.jse.2019.11.028.
25. Codispoti G, Carniato M, Brogini S, Romanelli A, Martini L, Giavaresi G, et al. Decellularized biological matrices for the repair of rotator cuff lesions: a systematic review of preclinical in vivo studies. Front Bioeng Biotechnol. 2024;12:1345343. https://doi.org/10.3389/fbioe.2024.1345343.
26. Roth SP, Brehm W, Groß C, Scheibe P, Schubert S, Burk J. Transforming growth factor Beta 3-Loaded decellularized equine Tendon Matrix for Orthopedic tissue Engineering. Int J Mol Sci. 2019;20. https://doi.org/10.3390/ijms20215474.
27. Pan J, Liu GM, Ning LJ, Zhang Y, Luo JC, Huang FG, et al. Rotator cuff repair using a decellularized tendon slices graft: an in vivo study in a rabbit model. Knee Surg Sports Traumatol Arthrosc. 2015;23:1524–35. https://doi.org/10.1007/s00167-014-2923-7.
28. Liu GM, Pan J, Zhang Y, Ning LJ, Luo JC, Huang FG, et al. Bridging repair of large rotator cuff tears using a multilayer decellularized tendon slices graft in a rabbit model. Arthroscopy. 2018;34:2569–78. https://doi.org/10.1016/j.arthro.2018.04.019.
29. Ferraris S, Pan G, Cassinelli C, Mazzucco L, Vernè E, Spriano S. Effects of sterilization and storage on the properties of ALP-grafted biomaterials for prosthetic and bone tissue engineering applications. Biomed Mater. 2012;7:054102. https://doi.org/10.1088/1748-6041/7/5/054102.
30. Potart D, Gluais M, Gaubert A, Da Silva N, Hourques M, Sarrazin M, et al. The cell-assembled extracellular matrix: a focus on the storage stability and terminal sterilization of this human bio material. Acta Biomater. 2023;166:133–46. https://doi.org/10.1016/j.actbio.2023.05.002.
31. de Sousa Iwamoto LA, Duailibi MT, Iwamoto GY, de Oliveira DC, Duailibi SE. Evaluation of ethylene oxide, gamma radiation, dry heat and autoclave sterilization processes on extracellular matrix of biomaterial dental scaffolds. Sci Rep. 2022;12:4299. https://doi.org/10.1038/s41598-022-08258-1.
32. Dearth CL, Keane TJ, Carruthers CA, Reing JE, Huleihel L, Ranallo CA, et al. The effect of terminal sterilization on the material properties and in vivo remodeling of a porcine dermal biologic scaffold. Acta Biomater. 2016;33:78–87. https://doi.org/10.1016/j.actbio.2016.01.038.
33. Jackson DW, Windler GE, Simon TM. Intraarticular reaction associated with the use of freeze-dried, ethylene oxide-sterilized bone-patella tendon-bone allografts in the reconstruction of the anterior cruciate ligament. Am J Sports Med. 1990;18:1–10. https://doi.org/10.1177/036354659001800101. discussion 10– 1.
34. Guo L, Yang L, Duan XJ, He R, Chen GX, Wang FY, et al. Anterior cruciate ligament reconstruction with bone-patellar tendon-bone graft: comparison of autograft, fresh-frozen allograft, and gamma-irradiated allograft. Arthroscopy. 2012;28:211–7. https://doi.org/10.1016/j.arthro.2011.08.314.
35. Issin A, Oner A, Sofu H, Yurten H. Comparison of freeze-dried tibialis anterior allograft and four-strand hamstring autograft in anterior cruciate ligament reconstruction. Acta Orthop Traumatol Turc. 2019;53:45–9. https://doi.org/10.1016/j.aott.2018.08.001.
36. Zouhair S, Aguiari P, Iop L, Vásquez-Rivera A, Filippi A, Romanato F, et al. Preservation strategies for decellularized pericardial scaffolds for off-the-shelf availability. Acta Biomater. 2019;84:208–21. https://doi.org/10.1016/j.actbio.2018.10.026.
37. Nieto-Nicolau N, López-Chicón P, Torrico C, Bolívar S, Contreras-Carreton E, Udina E, et al. Off-the-Shelf Nerve Matrix Preservation Biopreserv Biobank. 2022;20:48–58. https://doi.org/10.1089/bio.2020.0158.
38. Skornia A, Geerling G, Spaniol K, Witt J. Influence of Storage conditions on Decellularized Porcine Conjunctiva. Bioeng (Basel). 2023;10. https://doi.org/10.3390/bioengineering10030350.
39. Li N, Li Y, Gong D, Xia C, Liu X, Xu Z. Efficient decellularization for bovine pericardium with extracellular matrix preservation and good biocompatibility. Interact Cardiovasc Thorac Surg. 2018;26:768–76. https://doi.org/10.1093/icvts/ivx416.
40. Feichtinger X, Monforte X, Keibl C, Hercher D, Schanda J, Teuschl AH, et al. Substantial biomechanical improvement by extracorporeal Shockwave Therapy after Surgical repair of Rodent Chronic Rotator Cuff tears. Am J Sports Med. 2019;47:2158–66. https://doi.org/10.1177/0363546519854760.
41. Schanda JE, Keibl C, Heimel P, Monforte X, Tangl S, Feichtinger X, et al. Zoledronic acid substantially improves bone microarchitecture and Biomechanical properties after Rotator Cuff Repair in a Rodent Chronic defect model. Am J Sports Med. 2020;48:2151–60. https://doi.org/10.1177/0363546520926471.
42. Liu X, Manzano G, Kim HT, Feeley BT. A rat model of massive rotator cuff tears. J Orthop Res. 2011;29:588–95. https://doi.org/10.1002/jor.21266.
43. Shim IK, Kang MS, Lee ES, Choi JH, Lee YN, Koh KH. Decellularized bovine Pericardial Patch loaded with mesenchymal stromal cells enhance the mechanical strength and Biological Healing of large-to-massive Rotator Cuff tear in a rat model. Arthroscopy. 2022;38:2987–3000. https://doi.org/10.1016/j.arthro.2022.06.004.
44. Ide J, Kikukawa K, Hirose J, Iyama K, Sakamoto H, Fujimoto T, et al. The effect of a local application of fibroblast growth factor-2 on tendon-to-bone remodeling in rats with acute injury and repair of the supraspinatus tendon. J Shoulder Elb Surg. 2009;18:391–8. https://doi.org/10.1016/j.jse.2009.01.013.
45. Shah SA, Kormpakis I, Havlioglu N, Ominsky MS, Galatz LM, Thomopoulos S. Sclerostin antibody treatment enhances Rotator Cuff Tendon-to-bone Healing in an animal model. J Bone Joint Surg. 2017;99:855–64. https://doi.org/10.2106/jbjs.16.01019.
46. Rutala WA. APIC guideline for selection and use of disinfectants. Am J Infect Control. 1990;18:99–117. https://doi.org/10.1016/0196-6553(90)90089-b.
47. Monibi FA, Bozynski CC, Kuroki K, Stoker AM, Pfeiffer FM, Sherman SL, et al. Development of a Micronized Meniscus Extracellular Matrix Scaffold for potential augmentation of Meniscal Repair and Regeneration. Tissue Eng Part C Methods. 2016;22:1059–70. https://doi.org/10.1089/ten.TEC.2016.0276.
48. Wilson SL, Sidney LE, Dunphy SE, Dua HS, Hopkinson A. Corneal decellularization: a method of recycling unsuitable donor tissue for clinical translation? Curr Eye Res. 2016;41:769–82. https://doi.org/10.3109/02713683.2015.1062114.
49. Guimaraes AB, Correia AT, Alves BP, Da Silva RS, Martins JK, Pêgo-Fernandes PM, et al. Evaluation of a physical-chemical protocol for Porcine Tracheal Decellularization. Transpl Proc. 2019;51:1611–3. https://doi.org/10.1016/j.transproceed.2019.01.042.
50. McCrary MW, Vaughn NE, Hlavac N, Song YH, Wachs RA, Schmidt CE. Novel sodium deoxycholate-based Chemical decellularization method for peripheral nerve. Tissue Eng Part C Methods. 2020;26:23–36. https://doi.org/10.1089/ten.TEC.2019.0135.
51. Marrale J, Morrissey MC, Haddad FS. A literature review of autograft and allograft anterior cruciate ligament reconstruction. Knee Surg Sports Traumatol Arthrosc. 2007;15:690–704. https://doi.org/10.1007/s00167-006-0236-1.
52. Carey JL, Dunn WR, Dahm DL, Zeger SL, Spindler KP. A systematic review of anterior cruciate ligament reconstruction with autograft compared with allograft. J Bone Joint Surg Am. 2009;91:2242–50. https://doi.org/10.2106/jbjs.I.00610.
53. Singhal MC, Gardiner JR, Johnson DL. Failure of primary anterior cruciate ligament surgery using anterior tibialis allograft. Arthroscopy. 2007;23:469–75. https://doi.org/10.1016/j.arthro.2006.12.010.
54. Turner WD, Vasseur P, Gorek JE, Rodrigo JJ, Wedell JR. An in vitro study of the structural properties of deep-frozen versus freeze-dried, ethylene oxide-sterilized canine anterior cruciate ligament bone-ligament-bone preparations. Clin Orthop Relat Res 1988;251–6.
55. Mahirogullari M, Ferguson CM, Whitlock PW, Stabile KJ, Poehling GG. Freeze-dried allografts for anterior cruciate ligament reconstruction. Clin Sports Med. 2007;26:625–37. https://doi.org/10.1016/j.csm.2007.06.011.
56. Alarcon JF, Uribe-Echevarria B, Clares C, Apablaza D, Vargas JC, Benavente S, et al. Superior Capsular Reconstruction with Autologous Fascia Lata using a single lateral-row technique is an effective option in massive irreparable rotator cuff tears: Minimum 2-Year Follow-Up. Arthroscopy. 2021;37:2783–96. https://doi.org/10.1016/j.arthro.2021.04.009.
57. Bedi A, Bishop J, Keener J, et al. Rotator cuff tears. Nat Rev Dis Primers. 2024;10(1):8. https://doi.org/10.1038/s41572-024-00492-3. Published 2024 Feb 8.
58. Maffulli N, Nilsson Helander K, Migliorini F. Tendon appearance at imaging may be altered, but it may not indicate pathology. Knee Surg Sports

Traumatol Arthrosc. 2023;31(5):1625–8. https://doi.org/10.1007/s00167-023-07339-6.
59. Migliorini F, Maffulli N, Eschweiler J, Schenker H, Tingart M, Betsch M. Arthroscopic versus mini-open rotator cuff repair: a meta-analysis. Surgeon. 2023;21(1):e1–12. https://doi.org/10.1016/j.surge.2021.11.005.
60. Osti L, Del Buono A, Maffulli N. Rotator cuff repair: imaging success and clinical results may not correspond. Orthopedics. 2014;37(1):17–8. https://doi.org/10.3928/01477447-20131219-03.

Publisher's note